Hydroelastic Effects of Separated Flow

L. E. Ericsson*
Lockheed Missiles & Space Company, Inc., Sunnyvale, California

In a previous publication it was shown that separated flow can cause catastrophic divergent oscillations of an underwater structure that has a low drag cross-sectional profile. In the present paper the analysis is extended to rectangular prismatic sections, and to consider both bending and torsional oscillations. It is shown that the adverse hydroelastic effects of separated flow can be very large, requiring that a fix of some kind is used. Various means by which the hydroelastic instability can be avoided are described.

Nomenclature

b	= span
c	= two-dimensional chord length
d	= drag, coefficient $c_d = d/(\rho V^2/2)c$
E	= energy
F	= force
f	= frequency
h	= cross-sectional height
l	= sectional lift, coefficient, $c_l = 1/(\rho V^2/2)c$
$\tilde{m}$	= generalized mass
m_p	= sectional pitching moment, coefficient, $c_m = m_p/(\rho V^2/2)c^2$
n	= sectional normal force, coefficient, $c_n = n/(\rho V^2/2)c$
$P(t)$	= generalized force
q	= pitch rate
$q(t)$	= normalized coordinate
Re	= Reynolds number, $Re = Vc/\nu$
r	= corner radius
T	= torsional moment
t	= time
V	= cross flow velocity
$\bar{V}$	= reduced velocity, $\bar{V} = V/fh$
W	= work
x	= chordwise coordinate
y	= spanwise coordinate
z	= vertical coordinate (Fig. 5)
α	= angle of attack
Δ	= increment and amplitude
ζ_0	= structural damping, fraction of critical
$\zeta_a + \zeta_s$	= aerodynamic damping, fraction of critical
η	= dimensionless y coordinate, Eq. (9)
θ	= perturbation in pitch and torsion
ν	= kinematic viscosity
ξ	= dimensionless x coordinate, $\xi = x/c$
ξ_{sp}	= effect of separation point movement, Eq. (30)
ξ_w	= Kármán-Sears wake lag parameter, Eq. (30)
ρ	= fluid density
ϕ	= normalized modal deflection
ϕ_{LM}	= phase angle
ψ	= phase angle parameter, $\psi = \omega t$
$\omega, \bar{\omega}$	= oscillation frequency, $\omega = 2\pi f$; $\bar{\omega} = \omega c/V$

Subscripts

a	= attached flow
b	= bending
CR	= critical
d	= discontinuity
f	= forcing function
h	= hysteresis
MIN	= minimum
n	= numbering subscript, Eq. (9)
OC	= oscillation center and moment reference axis
s	= separated flow
sp	= separation point
t	= torsion
w	= wake
$1,2,3,\ldots$	= numbering subscripts

Superscripts

i	= separation-induced, e.g., $\Delta^i c_N$ = separation-induced normal force
$(\ )'$	= referenced to frontal area, e.g., $c_n' = n/(\rho V^2/2)h$

Derivative Symbols

$\dot{\alpha}$	$= \partial\alpha/\partial t$: $\ddot{q} = \partial^2 q/\partial t^2$
$c_{m\alpha}$	$= \partial c_m/\partial\alpha$: $c_{m_{\dot{z}}} = \partial c_m/\partial\left(\frac{\dot{z}}{V}\right)$
c_{mq}	$= \partial c_m/\partial\left(\frac{cq}{V}\right)$: $c_{m\dot{\alpha}} = \partial c_m/\partial\left(\frac{c\dot{\alpha}}{V}\right)$
$c_{m\dot{\theta}}$	$= c_{mq} + c_{m\dot{\alpha}}$
$c_{\bar{n}\dot{z}}$	= integrated mean value

Presented as Paper 82-0344 at the AIAA 20th Aerospace Sciences Meeting, Orlando, Fla., Jan. 11-14, 1982; submitted Jan. 22, 1982; revision received June 2, 1982.

*Senior Consulting Engineer. Associate Fellow AIAA.

Introduction

FIGURE 1 shows one of the cross-sectional geometries investigated for the Space Shuttle cable trays.[1,2] The rectangular cross section exhibits separation-induced negative lift characteristics[3] (Fig. 2; the c_m symbols are filled to distinguish them from the c_l symbols) similar to those for the profiled cross section discussed in Ref. 4 (Fig. 3). The main difference lies in the type of flow separation experienced. In Fig. 3 the separation proceeds from the trailing edge forward, whereas it starts at the sharp nose shoulder in Fig. 2. This causes the moment characteristics to be very different, although the lift or normal force characteristics are very similar. In Fig. 3 the negative lift is generated on the aft body, whereas it is produced near the nose of the rectangular cross section[2] (Fig. 4). Consequently, the rectangular cross section has a statically stabilizing moment around the elastic (mid-chord) axis, $c_{m\alpha} < 0$ at $\alpha = 0$, whereas the moment will be statically destabilizing (around the elastic axis) for the profile in Fig. 3. The hydroelastic consequence of this difference is that the streamlined profile will be subject to torsional (static) divergence, whereas the rectangle will experience divergent torsional oscillations. Both cross sections will exhibit divergent plunging or bending oscillations.

Analysis

The dynamics of the underwater structure are analyzed for oscillations both in bending and in torsion. The critical hydroelastic mechanisms for single degree-of-freedom oscillations in either bending or torsion are described in detail

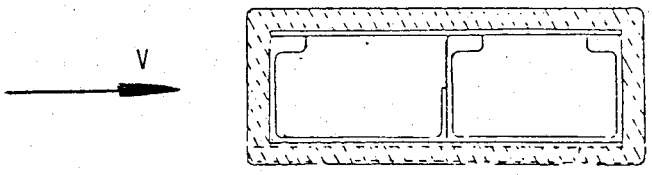

Fig. 1 Initial cable tray cross section.[2]

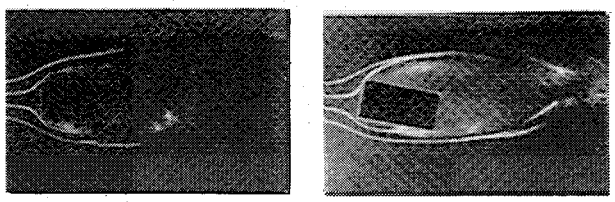

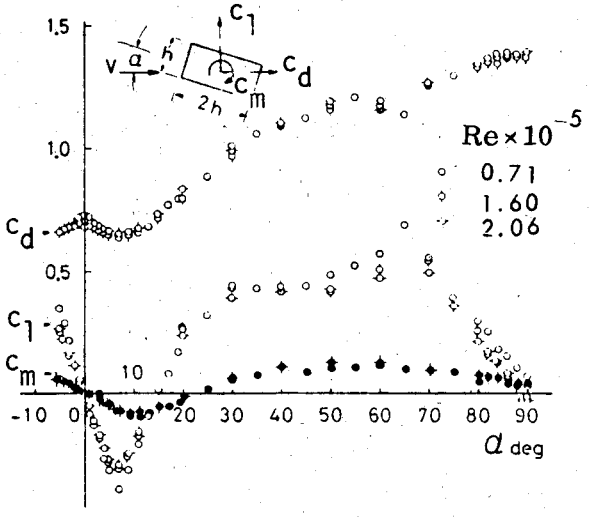

Fig. 2 Aerodynamic characteristics of a rectangular prism.[3]

and the unsteady hydrodynamics needed for a multi-degree-of-freedom analysis are developed.

The equations of motion can be written in the following form using standard notations

$$\tilde{m}[\ddot{q}(t)+2\zeta_0\omega\dot{q}(t)+\omega^2 q(t)]=P(t) \tag{1}$$

The generalized force $P(t)$ is given by the virtual work done by the aerodynamic forces and moments. (If W is the work done, $P=\partial W/\partial q$.)

For the bending degrees of freedom $P(t)$ is

$$P(t)=\int \frac{dF}{dy}\phi_b(y)\,dy \tag{2}$$

For the torsional degrees of freedom $P(t)$ becomes

$$P(t)=\int \frac{dT}{dy}\phi_t(y)\,dy \tag{3}$$

There are three different types of generalized force

$$P(t)=P_s(t)+P_a(t)+P_f(t) \tag{4}$$

where

$P_s(t)$ = generalized force in separated flow
$P_a(t)$ = generalized force in attached flow
$P_f(t)$ = generalized force independent of body motion, e.g., due to wake effects

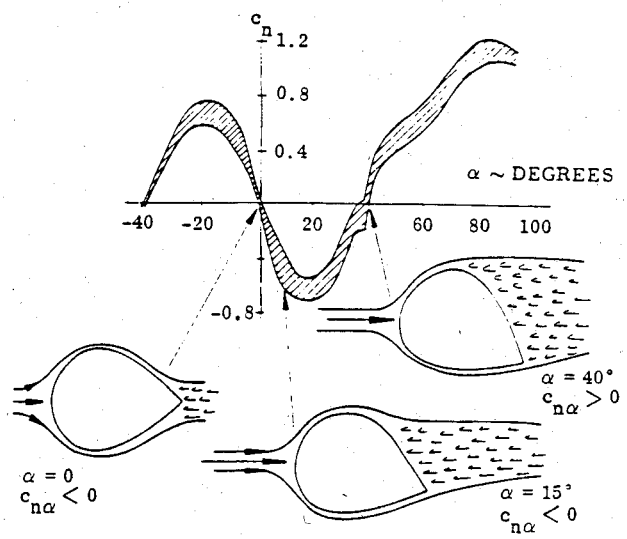

Fig. 3 Aerodynamic characteristics of a profiled cross section.[4]

While $P_a(t)$ and $P_f(t)$ usually can be defined by well established methods, $P_s(t)$ can often not be defined without a special analysis tailored to the problem at hand. Thus, the main effort is devoted to the description of $P_s(t)$.

Figure 5 shows the structural section in cross flow of velocity V. For small perturbations z/c and θ the sectional hydrodynamic force and moment induced by separated flow can be expressed in derivative form as follows, assuming that all surface-interference type terms, $c_n(z)$, associated with the depth z of the section below the surface, are negligible.

$$\frac{dF_s}{dy}=\frac{\rho V^2}{2}c\left[\Delta^i c_{n_\theta}\left(\theta+\frac{\dot{z}}{V}\right)+\Delta^i c_{n_{\dot\theta}}\frac{c\dot\theta}{V}+\Delta^i c_{n_{\ddot z}}\frac{c\ddot z}{V^2}+\Delta^i c_{n_{\ddot\theta}}\frac{c^2\ddot\theta}{V^2}\right]$$

$$\frac{dT_s}{dy}=\frac{\rho V^2}{2}c^2\left[\Delta^i c_{m_\theta}\left(\theta+\frac{\dot{z}}{V}\right)+\Delta^i c_{m_{\dot\theta}}\frac{c\dot\theta}{V}+\Delta^i c_{m_{\ddot z}}\frac{c\ddot z}{V^2}+\Delta^i c_{m_{\ddot\theta}}\frac{c^2\ddot\theta}{V^2}\right] \tag{5}$$

The corresponding expression for the attached flow derivative is

$$\frac{dF_a}{dy}=\frac{\rho V^2}{2}c\left[c_{n_\theta}\left(\theta+\frac{\dot{z}}{V}\right)+c_{n_{\dot\theta}}\frac{c\dot\theta}{V}+c_{n_{\ddot z}}\frac{c\ddot z}{V^2}+c_{n_{\ddot\theta}}\frac{c^2\ddot\theta}{V^2}\right]$$

$$\frac{dT_a}{dy}=\frac{\rho V^2}{2}c^2\left[c_{m_\theta}\left(\theta+\frac{\dot{z}}{V}\right)+c_{m_{\dot\theta}}\frac{c\dot\theta}{V}+c_{m_{\ddot z}}\frac{c\ddot z}{V^2}+c_{m_{\ddot\theta}}\frac{c^2\ddot\theta}{V^2}\right] \tag{6}$$

Equations (5) and (6) illustrate the hydrodynamic coupling between bending and torsional degrees of freedom. In addition, there may also be a structural coupling between these degrees of freedom.

In order to obtain an assessment of the danger potential of various hydroelastic mechanisms the underwater structure is first analyzed for one degree-of-freedom oscillations in either bending or torsion.

Bending Oscillations

For pure bending oscillations Eqs. (1-6) give the following results.

$$\ddot{q}_b(t)+2\omega_b(\zeta_0+\zeta_a+\zeta_s)\dot{q}_b(t)+\omega_b^2 q_b(t)=P_f(t)/\tilde{m}_b \tag{7}$$

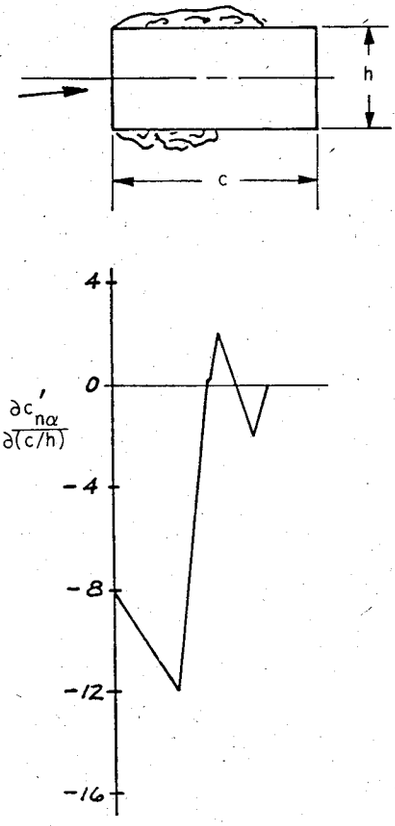

Fig. 4 Normal force derivative distribution on a rectangular prism.[2]

In a region of constant cross flow $\zeta_a + \zeta_s$ is defined as follows.

$$\zeta_a + \zeta_s = \frac{\rho V c}{4\omega_b \tilde{m}_b} (c_{n_\theta} + \Delta^i c_{n_\theta}) \int \phi_b^2(y)\,dy \tag{8}$$

Assuming that the constant cross flow extends over the "spanwise" distance b, Eq. (8) can be rewritten as

$$\zeta_a + \zeta_s = \frac{\rho V c b}{4\omega_b \tilde{m}_b} (c_{n_\theta} + \Delta^i c_{n_\theta}) \int_0^1 \phi_b^2(\eta)\,d\eta \tag{9}$$

where $\eta = (y - y_n)/(y_{n+1} - y_n)$ with $y_{n+1} - y_n = b$.

Hydrodynamic Damping

It can be seen from Eq. (7) that a necessary condition for bounded oscillations is the following:

$$\zeta_0 + \zeta_a + \zeta_s > 0 \tag{10}$$

where, for hydroelastic analysis, the structural damping ζ_0 usually is of negligible magnitude. Equation (10) shows that in absence of forcing functions, $P_f(t) = 0$, hydroelastic instability will only occur if the total normal force slope, $c_{n\alpha} = c_{n_\theta} + \Delta^i c_{n_\theta}$, is negative. The results obtained by Nakamura and Mizota[3] at incompressible speeds for a rectangular block of slenderness ratio $c/h = 2$ show that $c_{n\alpha} \approx c_{l\alpha} + c_d$ takes negative values at $\alpha < 8$ deg (Fig. 2). A systematic investigation of the characteristics of rectangular cross sections has been undertaken by Polhamus,[5] showing that large negative lift slopes exist at subcritical Reynolds number for chord-to-height ratios $c/h = 2/3$, 1, and 3/2. At supercritical Reynolds numbers large positive lift slopes are generated. Two characteristics stand out: 1) The supercritical $c_{n\alpha}$ value is reaching the thin plate value, $c_{n\alpha} = 2\pi$, even for $h/c > 1$. (Apparently, the increased drag makes up for the $c_{l\alpha}$ loss in composing $c_{n\alpha} \approx c_{l\alpha} + c_d$.) 2) When referenced to the frontal area (the profile height per unit span) the subcritical negative $c_{n\alpha}$ is of attached flow magnitude, i.e.,

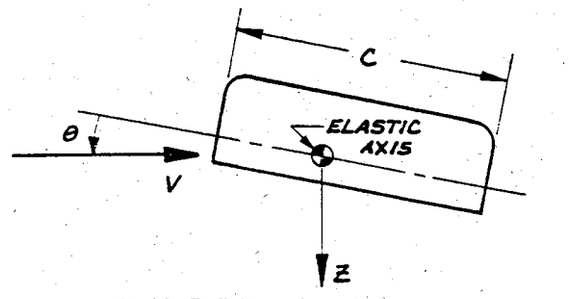

Fig. 5 Definition of coordinates.

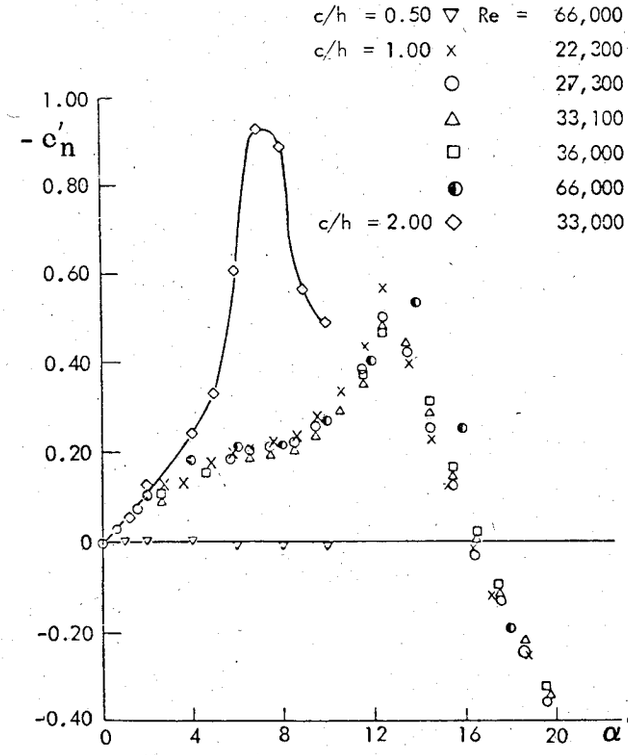

Fig. 6 Normal force characteristics of sharp-cornered rectangular cross sections.[9]

$$c_{n\alpha} \approx -2\pi h/c \tag{11}$$

Based upon these experimental results[3,5] (Fig. 2) one obtains the following definition of $c_{n\alpha}$.

$$\begin{aligned} c_{n\alpha} &= -2\pi h/c: \quad \alpha \le \alpha_d \\ &= 2\pi: \quad \alpha > \alpha_d \end{aligned} \tag{12}$$

Consequently, one needs to perform a nonlinear analysis to determine the damping for large amplitudes.

Nonlinear Damping Analysis

The nonlinear damping analysis in Ref. 6, which in turn is an extension of the methods presented in Refs. 7 and 8, will be modified to apply to the present case of bending oscillations. In the linear case the damping derivative $c_{n\dot{z}}$ is, simply,

$$-c_{n\dot{z}} = c_{n_\theta} + \Delta^i c_{n_\theta} = c_{n\alpha_s} \tag{13}$$

In the nonlinear case one can define a linear measure $c_{n\dot{z}}$ of the energy dissipation per oscillation cycle, which becomes $c_{n\dot{z}}$

when the nonlinearity disappears. For oscillations $z = |z|\sin\omega t$, where $c\omega/V = \bar{\omega}$, one obtains the following expressions for the energy dissipation per cycle (subscript b has been dropped from ω for simplicity).

$$E = \int c_n \mathrm{d}z = -c_{n_{\dot{z}}} \int \frac{\dot{z}}{V} \mathrm{d}z \tag{14}$$

That is,

$$-c_{n_{\dot{z}}} = \frac{\int_{t_0}^{t_0+2\pi/\omega} c_n \dot{z} \mathrm{d}t}{\int_{t_0}^{t_0+2\pi/\omega} \frac{\dot{z}}{V} \dot{z} \mathrm{d}t} = \frac{\int_{\psi_0}^{\psi_0+2\pi} c_n \cos\psi \mathrm{d}\psi}{\pi\bar{\omega}\Delta\zeta} \tag{15}$$

or

$$-c_{n_{\dot{z}}} = \frac{1}{\pi\bar{\omega}\Delta\zeta} \int_{\psi_0}^{\psi_0+2\pi} c_n \cos\psi \mathrm{d}\psi \tag{16}$$

Parkinson[9] used a seventh degree odd power polynomial to describe the nonlinear $c_n(\alpha)$ in Fig. 6. One can use a simpler representation through linear branches which probably will fit the data better than a polynomial.

$$\begin{aligned} c_n\left(\frac{\dot{z}}{V}\right) &= c_{n\alpha_1} \frac{\dot{z}}{V}; \qquad \left|\frac{\dot{z}}{V}\right| < \alpha_1 \\ &= c_{n\alpha_1}\alpha_1 + c_{n\alpha_2}\left(\frac{\dot{z}}{V} - \alpha_1\right); \quad \alpha_1 \le \left|\frac{\dot{z}}{V}\right| < \alpha_2 \\ &= c_{n\alpha_1}\alpha_1 + c_{n\alpha_2}(\alpha_2 - \alpha_1) \\ &\quad + c_{n\alpha_3}\left(\frac{\dot{z}}{V} - \alpha_2\right); \quad \left|\frac{\dot{z}}{V}\right| \ge \alpha_2 \end{aligned} \tag{17}$$

Combining Eqs. (16) and (17) gives

$$\begin{aligned} -c_{n_{\dot{z}}} &= c_{n\alpha_1} + \frac{2}{\pi}(c_{n\alpha_2} - c_{n\alpha_1})\left[\arccos\left(\frac{\alpha_1}{\Delta\zeta\bar{\omega}}\right)\right. \\ &\quad \left. - \frac{\alpha_1}{\Delta\zeta\omega}\sqrt{1-\left(\frac{\alpha_1}{\Delta\zeta\bar{\omega}}\right)^2}\right] + \frac{2}{\pi}(c_{n\alpha_3} - c_{n\alpha_2})\left[\arccos\left(\frac{\alpha_2}{\Delta\zeta\bar{\omega}}\right)\right. \\ &\quad \left. - \frac{\alpha_2}{\Delta\zeta\bar{\omega}}\sqrt{1-\left(\frac{\alpha_2}{\Delta\zeta\bar{\omega}}\right)^2}\right] \end{aligned} \tag{18}$$

Comparing the results in Fig. 6 with those in Fig. 2 one obtains the situation sketched in Fig. 7. It appears that the results by Nakamura and Mizota[2] (Fig. 2) represent one limiting case for Parkinson's data[9] (Fig. 6). The other limit is shown by a dashed line. Using only two linear branches, the dash-dot curve in Fig. 7, one has to set $c_{n\alpha_1} = 0$ and $\alpha_1 = 0$ in Eq. (16), with the following result.

$$\begin{aligned} -c_{n_{\dot{z}}} &= \frac{c_{n_{\mathrm{MIN}}}}{\alpha_2} + \frac{2}{\pi}\left(c_{n\alpha_3} - \frac{c_{n_{\mathrm{MIN}}}}{\alpha_2}\right) \\ &\quad \times \left[\arccos\left(\frac{\alpha_2 V}{\Delta z\omega}\right) + \left(\frac{\alpha_2 V}{\Delta z\omega}\right)\sqrt{1-\left(\frac{\alpha_2 V}{\Delta z\omega}\right)^2}\right] \end{aligned} \tag{19}$$

In the other limit, where $c_{n\alpha_2} \to 0$ and $c_{n\alpha_2}\alpha_2 \to c_{n_{\mathrm{MIN}}}$, Eq. (19) becomes

$$-c_{n_{\dot{z}}} = \frac{2c_{n\alpha_3}}{\pi}\left[\arccos\left(\frac{\alpha_2 V}{\Delta z\omega}\right) + \left(\frac{\alpha_2 V}{\Delta z\omega}\right)\sqrt{1-\left(\frac{\alpha_2 V}{\Delta z\omega}\right)^2}\right]$$

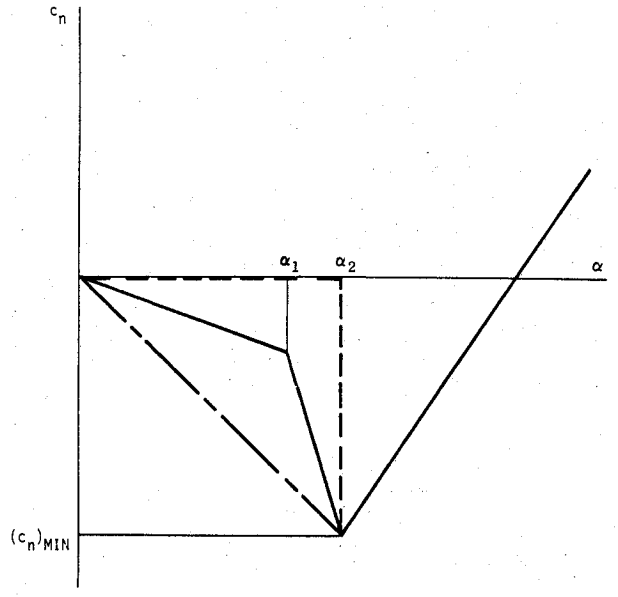

Fig. 7 Candidate nonlinear normal force characteristics of rectangular cross sections.

$$-\frac{4}{\pi}\left(c_{n\alpha_3} - \frac{c_{n_{\mathrm{MIN}}}}{\alpha_2}\right)\left(\frac{\alpha_2 V}{\Delta z\omega}\right)\sqrt{1-\left(\frac{\alpha_2 V}{\Delta z\omega}\right)^2} \tag{20}$$

For the rectangular cross sections in Fig. 6 one obtains

$$\begin{aligned} c/h = 2: \quad & c_{n\alpha_1} = -1.75, \quad c_{n\alpha_2} = -9.75 \\ & c_{n\alpha_3} = 6.5, \quad c_{n_{\mathrm{MIN}}} = -0.50 \\ & \alpha_1 = 5.1 \text{ deg} = 0.089 \\ & \alpha_2 = 6.8 \text{ deg} = 0.119 \\ c/h = 1: \quad & c_{n\alpha_1} = -1.6, \quad c_{n\alpha_2} = -4.5 \\ & c_{n\alpha_3} = 6.5, \quad c_{n_{\mathrm{MIN}}} = -0.50 \\ & \alpha_1 = 9 \text{ deg} = 0.17 \\ & \alpha_2 = 13 \text{ deg} = 0.226 \end{aligned} \tag{21}$$

Combining Eqs. (18-21) gives the results shown in Fig. 8. It can be seen that the value $|\dot{z}|/V$ for $c_{n_{\dot{z}}} = 0$, which is the plunging limit cycle amplitude for $\zeta_0 = 0$, is not very sensitive to the detailed damping characteristics at $0 \le |\dot{z}|/V \le \alpha_2$, a result in basic agreement with past experience for axisymmetric blunt nosed bodies, limit cycling in pitch.[7] It would appear that the simple Eq. (10) would suffice, especially in view of the results in Fig. 2. Figure 9 shows that this prediction is in reasonable agreement with experiment.[9] As the tests were performed with nonzero mechanical damping, $\zeta_0 > 0$, the predictions should be higher than the experimental data.

All the results discussed so far have neglected the effect of the forcing function, $P_f(t)$ in Eq. (1). It is well known that the rectangular cross section will shed a Kármán type of vortex wake. Less well known is its effect on the limit cycle amplitude.

Vortex Wake Effects

Nakamura and Mizota[10] have performed a detailed investigation of the wake effects on the unsteady aerodynamics of sharp-edged rectangular prisms. Their test was performed at incompressible speeds, $V \le 12.2$ m/s (40 ft/s) and the effect of $\bar{V} = V/fh$ on the amplitude response in Fig. 10 represents

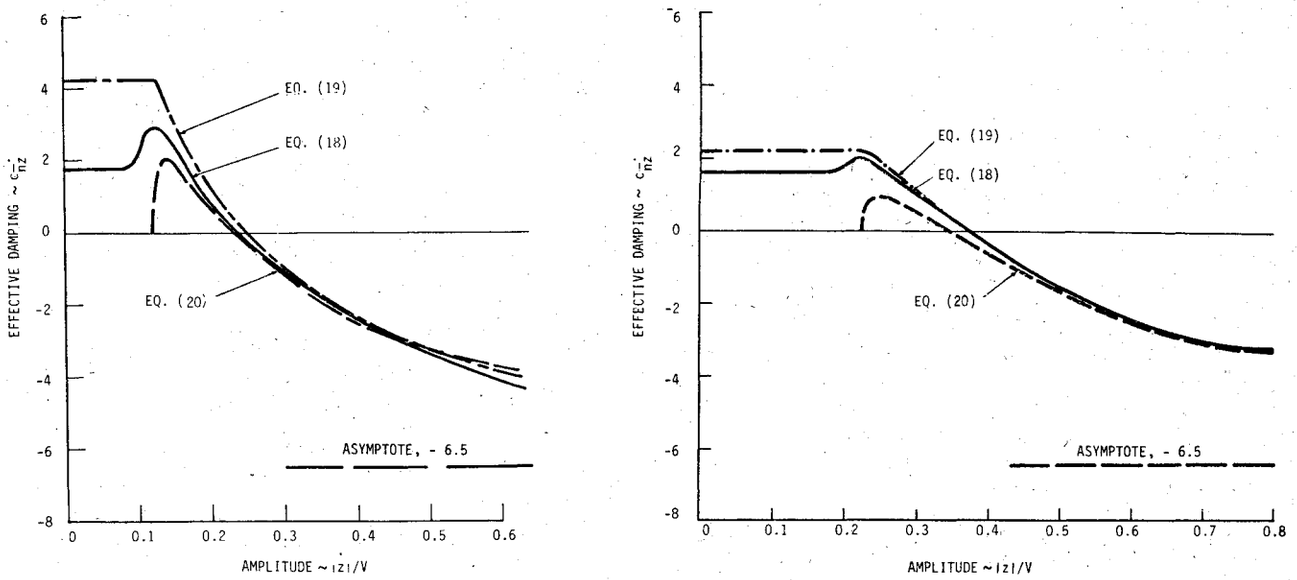

Fig. 8 Nonlinear damping characteristics of rectangular prisms.

solely a frequency effect. One finds that a $c/h=1$ prism exhibits limit cycle behavior† at large $\bar{V}$, in agreement with Parkinson's results[9] (Fig. 9). The data show that the prism starts to build up an amplitude response when $\bar{V}$ is slightly above the critical value for the basic Kármán vortex shedding, i.e., when the frequency is slightly below the vortex shedding frequency, in agreement with the amplitude response behavior observed by Jones et al.[11] The measured phase angle (Fig. 11) illustrates further how the cross-sectional response develops from vortex induced to self induced. Again one notices that in agreement with the results of Jones et al.[11] the phase angle goes from being damping at $\bar{V}<\bar{V}_{CR}$ to becoming undamping at $\bar{V}>\bar{V}_{CR}$. When $\bar{V}$ is increased far above $\bar{V}_{CR}$ the phase angle approaches asymptotically the 90-deg value corresponding to the self-excited large-amplitude response.

Torsional Oscillations

For pure torsional oscillations Eqs. (1-6) give the following results.

$$\ddot{q}(t)+2\omega_t(\zeta_0+\zeta_a+\zeta_s)\dot{q}(t)+\omega_t^2 q(t)=[P_f(t)/\tilde{m}_t] \quad (22)$$

In a region of constant cross flow $\zeta_a+\zeta_s$ is defined as follows.

$$\zeta_a+\zeta_s=-\frac{Vc^3}{4\omega_t\tilde{m}_t}(c_{m\dot{\theta}}+\Delta^i c_{m\dot{\theta}})\int\phi_t^2(y)\,dy \quad (23)$$

With η defined as before in Eq. (9), one can write Eq. (23) as follows.

$$\zeta_a+\zeta_s=-\frac{\rho Vc^3 b}{4\omega_t\tilde{m}_t}(c_{m\dot{\theta}}+\Delta^i c_{m\dot{\theta}})\int_0^1\phi_t^2(\eta)\,d\eta \quad (24)$$

†Note that $|\dot{z}|/V=\text{const}$ implies that $\Delta z/h=(\text{const}/2\pi)\bar{V}$, corresponding to the constant slopes approached asymptotically for large $\bar{V}$ in Fig. 10.

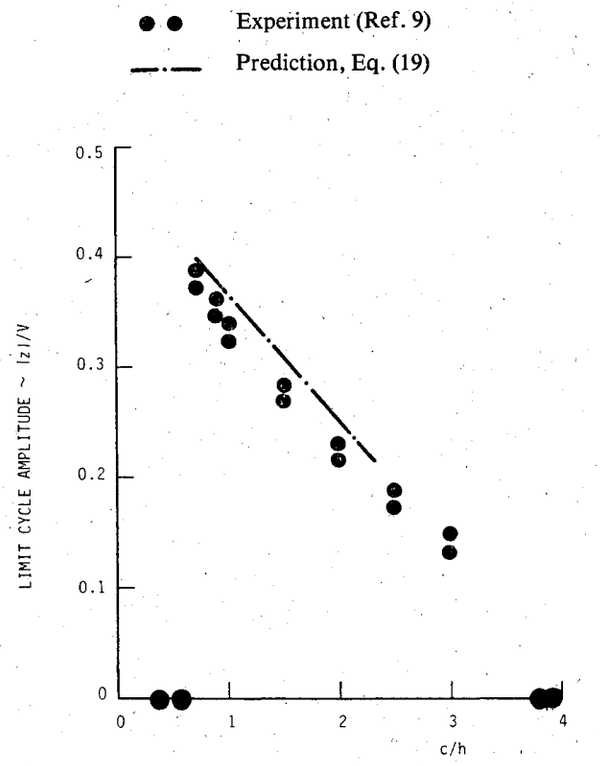

Fig. 9 Limit cycle amplitude of rectangular prisms describing plunging oscillations.

Hydrodynamic Damping

Studying the pressure distribution on rectangular cross sections[9,12] the load distribution shown in Fig. 4 was obtained[2] (the "primed" coefficient is based on the frontal area rather than on the horizontal area). Combining this distribution with the $c_{n\alpha}$ data gives the needed $c_{m\alpha}$ data at low speeds.

$$c_{m\alpha}=c_{m_\theta}+\Delta^i c_{m_\theta} \quad (25)$$

c_{m_θ} is the attended flow value and $\Delta^i c_{m_\theta}$ the effect of

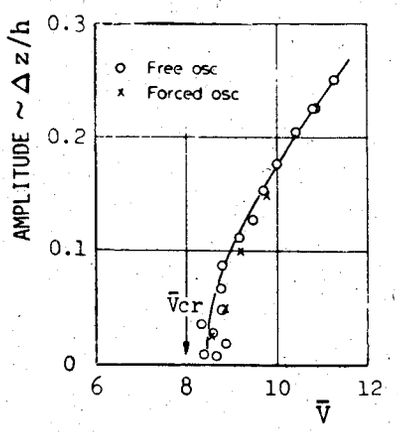

Fig. 10 Amplitude response of a $c/h=1$ rectangular prism.[12]

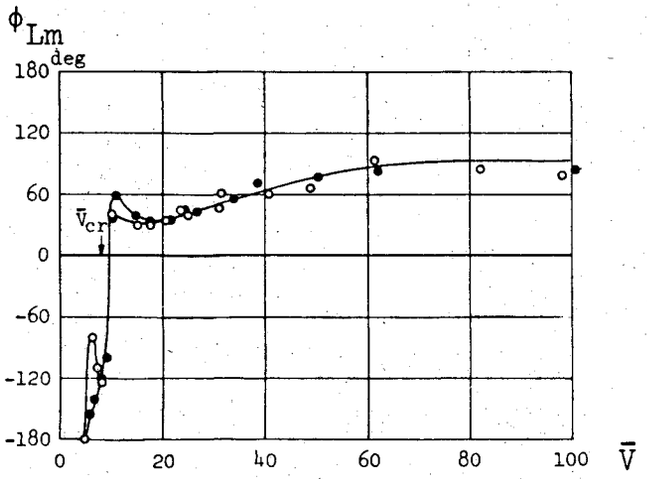

Fig. 11 Phase angle for the response of a $c/h=1$ rectangular prism.[12]

separated flow. Using thin airfoil theory one obtains

$$c_{m_\theta} = -2\pi(0.25 - \xi_{OC}) \tag{26}$$

In similarity to Eq. (25) one can express the torsional damping derivative as follows.

$$c_{m_{\dot\theta_t}} = c_{m_{\dot\theta}} - \tau_s \Delta c_{m_{\dot\theta_s}} \tag{27}$$

The attached flow damping is simply[14,15]

$$c_{m_{\dot\theta}} = 2\pi[\xi_w(0.25 - \xi_{OC}) - 0.25(\xi_{OC} - 0.75)] \tag{28}$$

where

$$\xi_w = 1.5: \ \bar\omega \le 0.16$$
$$= 0.245/\bar\omega: \ \bar\omega > 0.16 \tag{29}$$

The separated flow time lag parameter τ_s is[13,14]

$$\tau_s = \xi_w + \xi_{sp}$$
$$\xi_w = 1.5$$
$$\xi_{sp} = 0: \text{ sharp L.E.}$$
$$= 0.75: \text{ rounded L.E.} \tag{30}$$

Combining Eqs. (25-30) one can compute the torsional damping measured on a rectangular cross section. The

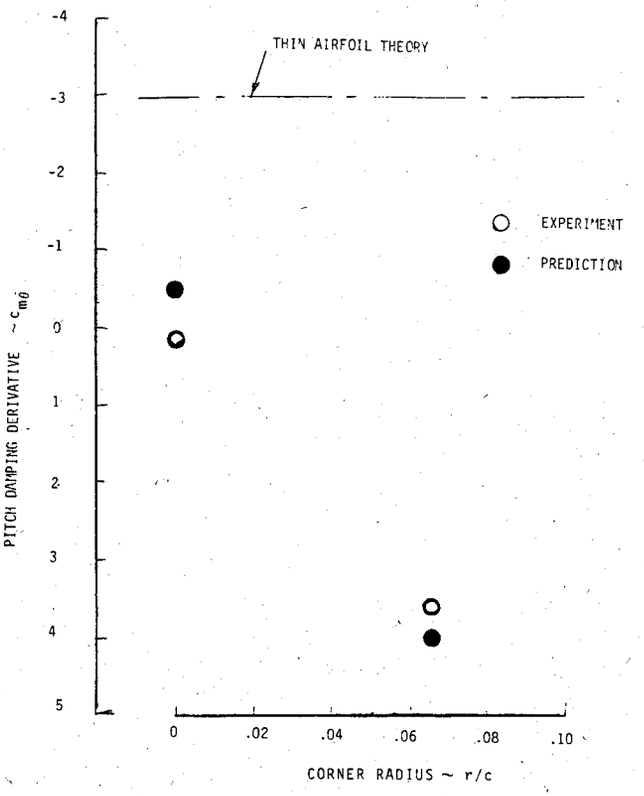

Fig. 12 Predicted and measured pitch damping of a rectangular prism with sharp and rounded corners.

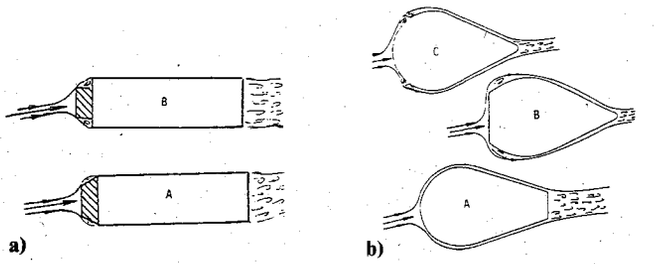

Fig. 13 Fluid dynamic fixes employing the preseparation concept a) rectangular cross sections and b) profiled cross sections.

predictions for $c/h=2$ rectangular cross sections with sharp and rounded corners are compared in Fig. 12 with experimental results.[15,16] The agreement is remarkably good, considering that the analytic theory[13,14] was developed for cross sections that are much thinner than the blunt rectangular prism. The results in Fig. 12 reveal that as soon as the rectangular cross section deviates from the sharp-edged geometry that "locks" the location of flow separation at the leading edge, large dynamically destabilizing moment derivatives are generated. The consequence will be divergent torsional oscillations of the underwater structure, as the structural or mechanical damping usually is of negligible magnitude compared to the hydrodynamic value, $|\zeta_0| \ll |\zeta_a + \zeta_s|$.

Thus, in order to assure hydroelastic torsional stability of a structure with rectangular cross section one has to use some means by which the flow separation effects can be alleviated or possibly eliminated. In regard to the divergent oscillations in plunge and bending discussed earlier it is not only the rectangular cross section that causes hydroelastic instability, but a rather broad range of both bluff and slender profiles.[17] Thus, there is a general need for a fluid dynamic fix of some type. One type which requires relatively modest changes of the

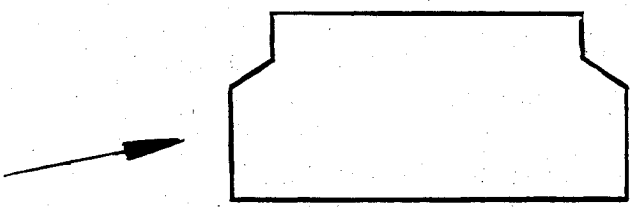

Fig. 14 Final cable tray cross section.[2]

cross-sectional geometry uses the "preseparation" concept,[6] in which an early local flow separation is induced in order to avoid a more extensive one further downstream. Examples of such fixes for drop-shaped and rectangular cross sections are shown in Fig. 13. Confirmation of the effectiveness of the indented rectangular shape (section B in Fig. 13b) was obtained quite by chance in recent tests[15,16] of the shape shown in Fig. 14, where the indentation had completely nonfluid-dynamic reasons.

Conclusions

The results of an analysis of hydroelastic effects of separated flow can be summarized as follows.

1) Bending and plunging oscillations are hydroelastically unstable for a large family of cross-sectional shapes with varying "bluffness."

2) Rectangular cross sections often will be hydroelastically unstable in torsion.

3) Fluid dynamic fixes of the "preseparation" type can alleviate and possibly eliminate the adverse hydroelastic effects of separated flow.

References

[1]Ericsson, L. E. and Reding, J. P., "Aeroelastic Stability of Space Shuttle Protuberances," *Journal of Spacecraft and Rockets*, Vol. 19, July-Aug. 1982, pp. 307-313.

[2]Ericsson, L. E. and Reding, J. P., "Aeroelastic Analysis of the Space Shuttle External Tank Cable Trays," Final Tech. Rept. LMSC-D766543, Contract ASO-751485, April 1981.

[3]Nakamura, Y. and Mizota, T., "Aerodynamic Characteristics and Flow Patterns of a Rectangular Block," *Reports of Research Institute for Applied Mechanics*, Kyushu University, Japan, Vol. XIX, No. 65, March 1972, pp. 289-294.

[4]Ericsson, L. E. and Reding, J. P., "Potential Hydroelastic Instability of Profiled Underwater Structures," *Journal of Hydronautics*, Vol. 14, Oct. 1980, pp. 97-104.

[5]Polhamus, E. C., "Effect of Flow Incidence and Reynolds Number on Low-Speed Aerodynamic Characteristics of Several Noncircular Cylinders with Applications to Directional Stability and Spinning," NASA TR R-29, 1959.

[6]Ericsson, L. E., "Aeroelastic Instability Caused by Slender Payloads," *Journal of Spacecraft and Rockets*, Vol. 1, Jan. 1967, pp. 65-73.

[7]Ericsson, L. E., "Separated Flow Effects on the Static and Dynamic Stability of Blunt Nosed Cylinder Flare Bodies," NASA CR 76919, Dec. 1965.

[8]Ericsson, L. E., "Unsteady Aerodynamics of Separating and Reattaching Flow on Bodies of Revolution," *Recent Research on Unsteady Boundary Layers*, Vol. 1, IUTAM Symposium, Laval University, Quebec, May 1971, pp. 481-512.

[9]Parkinson, G. V., "Aeroelastic Galloping in One Degree of Freedom," *Proceedings of the Conference on Wind Effects on Buildings and Structures*, National Physics Laboratory, England, June 1963, Vol. II, London, 1965, pp. 582-609.

[10]Nakamura, Y. and Mizota, T., "Unsteady Lifts and Wakes of Oscillating Rectangular Prisms," *Journal of Engineering Mechanical Division, Proceedings of the ASCE*, Vol. 101, No. EM6, Dec. 1975, pp. 858-871.

[11]Jones, G. W. Jr., Cincotta, J. C., and Walker, R. W., "Aerodynamic Forces on a Stationary and Oscillating Circular Cylinder at High Reynolds Number," NASA TR R-300, Feb. 1969.

[12]Nakamura, Y. and Tomonari, Y., "Pressure Distributions on Rectangular Prisms at Small Incidence," *Transactions, Japan Society for Aeronautical and Space Sciences*, Vol. 21, No. 54, 1979, pp. 205-213.

[13]Ericsson, L. E. and Reding, J. P., "Unsteady Airfoil Stall, Review and Extension," *Journal of Aircraft*, Vol. 8, Aug. 1971, pp. 609-616.

[14]Ericsson, L. E. and Reding, J. P., "Dynamic Stall Analysis in Light of Recent Numerical and Experimental Results," *Journal of Aircraft*, Vol. 13, April 1976, pp. 248-255.

[15]LaBerge, J. G., "Dynamic Wind Tunnel Tests of the Shuttle External Tank Cable Trays at Subsonic Speeds," LTR-UA-55, Feb. 1981.

[16]Orlik-Rückemann, K. J. and LaBerge, J. G., "Dynamic Wind Tunnel Tests of the Simulated Shuttle External Tank Cable Trays," AIAA Paper 81-1879, Aug. 1981.

[17]Ericsson, L. E., "Limit Amplitude of Galloping Cables," AIAA Paper 83-0132, Jan. 1983.